



# Vacancy-mediated ferromagnetism in Co-implanted ZnO studied using a slow positron beam

D. D. Wang<sup>1,2</sup>, B. Zhao<sup>2</sup>, N. Qi<sup>2</sup>, Z. Q. Chen<sup>2,\*</sup>, and A. Kawasuso<sup>3</sup>

<sup>1</sup> School of Physics and Engineering, Henan University of Science and Technology, Luoyang 471023, China

<sup>2</sup> Hubei Nuclear Solid Physics Key Laboratory, Department of Physics, Wuhan University, Wuhan 430072, China

<sup>3</sup> Advanced Science Research Center, Japan Atomic Energy Agency, 1233 Watanuki, Takasaki, Gunma 370-1292, Japan

Received: 10 October 2016

Accepted: 20 February 2017

Published online:

2 March 2017

© Springer Science+Business Media New York 2017

## ABSTRACT

Co<sup>+</sup> ions with multiple energies from 50 to 380 keV were implanted into ZnO single crystals up to a total dose of  $1.25 \times 10^{17} \text{ cm}^{-2}$ . The implanted samples were annealed in open air for 30 min between 200 and 1100 °C. All the samples before and after implantation and annealing were characterized by X-ray diffraction (XRD), Raman scattering and positron annihilation measurements. XRD and Raman scattering measurements indicate that Co implantation induces severe lattice damage, and after annealing the damage recovers gradually. No Co clusters or Co-related second phase was observed in the implanted samples. Doppler broadening of positron annihilation radiation measurements using a slow positron beam reveals a large number of vacancy clusters introduced by Co implantation. After annealing up to 1000 °C, almost all the defects induced by implantation are removed. The implanted samples show clear ferromagnetism measured at 5 K. It shows very slight decrease after annealing at 700 °C and becomes much weaker after annealing at 1000 °C. The origin of ferromagnetism is most probably due to substitution of Co<sup>+</sup> ions at Zn lattice sites. However, it is apparent that the decrease in magnetization after annealing is consistent with the vacancy recovery process, indicating that the ferromagnetism in Co-implanted ZnO is mediated by defects such as Zn vacancy ( $V_{\text{Zn}}$ ) or vacancy clusters. First principles calculations also support that Zn-related monovacancies and vacancy clusters can enhance the ferromagnetism in Co-doped ZnO.

## Introduction

Magnetic semiconductors have attracted considerable attention due to their potential applications in spin electronic devices. They provide an excellent material system for investigating the concepts of

semiconductor-based spintronic devices, which utilize both charge and spin of electrons [1, 2]. Since Dietl et al. [3] first predicted that Mn-doped p-type ZnO and GaN leads to high-Curie-temperature ferromagnetism, many researchers have tried various attempts to dope semiconductors with transition

Address correspondence to E-mail: chenzq@whu.edu.cn

metals to obtain dilute magnetic semiconductors (DMSs) [4, 5]. Numerous experimental groups reported ferromagnetism at room temperature in transition metal-doped ZnO and GaN, using various methods such as ion implantation, [6, 7] sol-gel, [8] pulsed laser deposition (PLD), [9] MOCVD, [10].

Some fundamental problems about dilute magnetic semiconductors still remain unsolved. A key issue is the origin of magnetism in these materials. Numerous research works about the ferromagnetism in transition metal-doped ZnO have been reported, but the origin of ferromagnetism has not been fully understood. Some researchers proposed that ferromagnetism may be due to magnetic impurity clusters or the second phase, while others suggested that the ferromagnetism is intrinsic which is due to substitution of transition metal atoms at the Zn lattice site. Recently in undoped ZnO thin films and nanoparticles, ferromagnetism was also observed, which was suggested to be induced by defects such as Zn vacancies or O vacancies [11–15]. This adds new explanations for the ferromagnetism. In transition metal-doped ZnO, defects are also suggested to enhance the ferromagnetism [16–24]. However, there is no consensus on which kind of defect is responsible for the enhancement of the ferromagnetism. Actually the evidence for defect enhanced magnetism is also not so strong, since the defects are usually characterized by Raman and photoluminescence measurements, which can only give indirect information about defects. Identification of defects in ZnO by Raman and photoluminescence is still controversial. A more convincing method is thus needed to investigate the correlation between defects and ferromagnetism in transition metal-doped ZnO.

Cobalt is a common 3d transition metal which is expected to induce ferromagnetism in ZnO. Since the radius of a  $\text{Co}^+$  ion ( $r = 72$  pm) in tetrahedral coordination is very close to that of a  $\text{Zn}^+$  ion ( $r = 74$  pm), [25] the Co atoms should preferentially occupy Zn sites. Lee et al. [26] and Rode et al. [27] reported intrinsic ferromagnetism in Co-doped ZnO films with a Curie temperature of approximately 350 K. Ueda et al. [9] also observed ferromagnetism above room temperature in Co-doped ZnO. However, there have also been many results which reported the absence of ferromagnetism in Co-doped ZnO [28–31]. This suggests that the magnetic properties of Co-doped ZnO are very sensitive to the sample preparation condition. It seems that occupation of Zn lattice sites by

transition metals is not sufficient to introduce ferromagnetism. The role of defects on the magnetic coupling in Co-doped ZnO cannot be neglected.

Ion implantation is a suitable doping technique in semiconductors. It can introduce transition metal ions into ZnO in the selected area with high accuracy and good repeatability [32–38]. However, a large quantity of defects will be also introduced in the implanted layer and will affect the optoelectronic and magnetic properties. It is therefore of great importance to study the transition metal ion implantation-induced defects in ZnO and the effect of defects on the ferromagnetism.

Positron annihilation spectroscopy is a powerful tool to study microstructure in materials. It is particularly sensitive to the atomic-scale vacancy-type defects. Due to the repulsion between positrons and the positively charged ion cores, positrons prefer to be trapped by vacancies where atoms are missing. The positron annihilation parameters such as annihilation lifetime and Doppler broadening of annihilation radiation at vacancy sites will be quite different from those annihilated at perfect lattice site. Therefore, identification of vacancy defects by positrons is very straightforward. The slow positron technique is particularly suitable for the study of implantation-induced defects near the surface and subsurface region. By changing positron incident energy, the depth distribution of defects can be obtained. Positron annihilation spectroscopy has been successfully applied to study grown-in defects as well as electron irradiation and ion implantation-induced defects in ZnO [39–42].

In this paper, we incorporated Co into ZnO by the implantation technique. The implantation-induced defects and their thermal stability were studied by positron annihilation measurements using a slow positron beam. X-ray diffraction and Raman scattering measurements were also performed for comparison. Our measurements reveal that positron annihilation is very sensitive to the defect production and recovery process in implanted ZnO, and the Co-doping-induced ferromagnetism is closely correlated with the implantation-induced defects.

## Experiment

Hydrothermal-grown undoped ZnO single crystals with dimensions of  $10 \times 10 \times 0.5$  mm<sup>3</sup> were purchased from Hefei Kejing Materials Technology

Corporation. The samples were grown along the  $\langle 0001 \rangle$  orientation and were single-side polished on the Zn-terminated surface.  $\text{Co}^+$  ions implantation was carried out using a 400 keV ion implanter in Japan Atomic Energy Agency (JAEA). A multiple-step implantation process was carried out with ion energies from 50 to 380 keV. The implantation was carried out from low to high energy in turn.  $\text{Co}^+$  ions were implanted to the polished (Zn) face of the samples. Beam fluxes were about  $1.2 \times 10^{13} \text{ cm}^{-2} \text{ s}^{-1}$ . The total dose of implanted  $\text{Co}^+$  ions was  $1.25 \times 10^{17} \text{ cm}^{-2}$ . The implanted ion profile was calculated by the TRIM code, which is based on Monte Carlo method [43]. As shown in Fig. 1, a box-shaped implantation profile with a thickness of about 220 nm was formed after this multiple-step implantation. The atomic density in the implanted layer is about  $5 \times 10^{17} \text{ cm}^{-2}$ , which corresponds to a Co concentration of about 6 at.%. The implanted samples were annealed in open air at temperatures ranging from 100 to 1000 °C for 30 min at each temperature.

All the samples were characterized by X-ray diffraction (Bruker D8 Advance diffractometer, Germany) using  $\text{CuK}\alpha$  radiation ( $\lambda = 0.15418 \text{ nm}$ ). The scanning range was from  $30^\circ$  to  $75^\circ$ , and the increment was  $0.01^\circ$ . Micro-Raman scattering spectra (Renishaw RM-1000 Confocal micro-Raman spectroscopy, England) excited with the 515 nm line of an  $\text{Ar}^+$  laser were recorded in backscattering geometry with a power level of about 4.8 mW arriving at the sample surface. The scanning wave numbers of Raman shift ranged from 200 to  $800 \text{ cm}^{-1}$ . The magnetization versus applied magnetic field was measured using a DC superconducting quantum

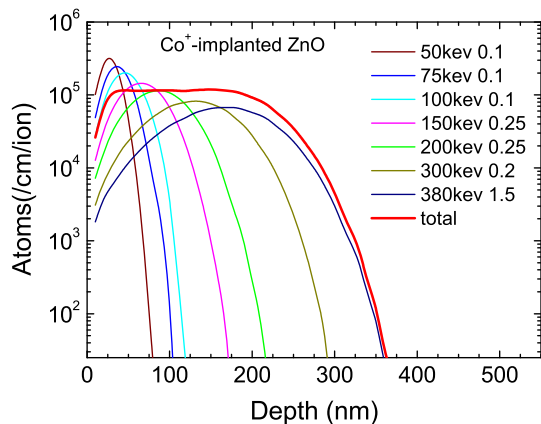


**Figure 1** TRIM simulation of the depth profile of implanted ions for ZnO after multiple-step  $\text{Co}^+$  implantation.

interference device (SQUID, Quantum Design PPMS) magnetometer. The measurements were taken at low temperature of 5 K.

Doppler broadening of positron annihilation radiation was measured using a high-purity Ge detector. A slow positron beam with variable positron energy ranging from 0.2 to 30 keV was used. The conventional  $S$  and  $W$  parameter is used to quantitatively characterize the Doppler broadening spectrum, which are defined as the ratio of the counts in the central peak region ( $511 \pm 0.76 \text{ keV}$ ) and wing region ( $511 \pm 3.4$  to  $511 \pm 6.8 \text{ mkeV}$ ) to the total area of the annihilation peak, respectively. When a positron is trapped at a vacancy site, the probability of positron annihilation with high momentum core electrons is reduced, so the Doppler broadening spectrum becomes narrower, and the  $S$  parameter increases.

## Results and discussion

Figure 2 shows the XRD pattern of ZnO before and after  $\text{Co}^+$ -implantation and annealing. All the samples show two peaks at around  $34.5^\circ$  and  $72.5^\circ$ , which correspond to the (002) and (004) diffraction peaks of ZnO. This implies that the implantation and

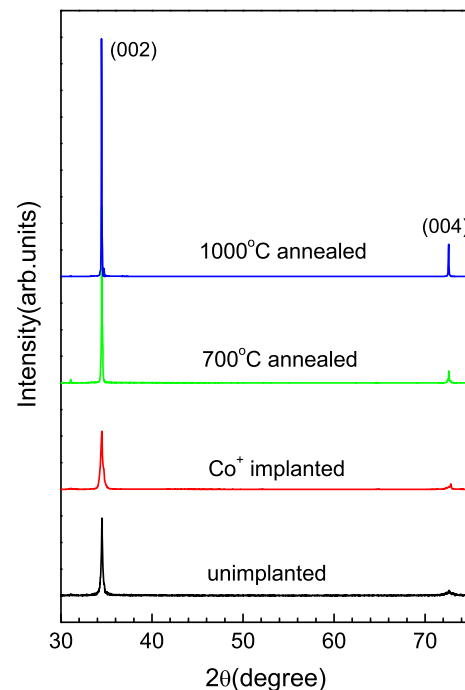


**Figure 2** XRD pattern of  $2\theta$  scans for ZnO before and after Co implantation and annealing at different temperatures.

subsequent thermal treatment do not change the wurtzite structure of ZnO. After  $\text{Co}^+$  implantation, the crystal quality deteriorates drastically, since both the two diffraction peaks become much wider. This suggests that  $\text{Co}^+$  implantation introduces a large number of defects in the implanted layer. After annealing, the implantation-induced defects gradually recover, as the diffraction peak becomes narrower. The thermal treatment will drive atoms which were deviated by the implantation to rearrange the order in the crystal. After annealing above  $700^\circ\text{C}$ , the (002) diffraction peak is even narrower than the unimplanted sample, indicating that the implantation damage has been removed by annealing, and the crystal quality becomes better than the as-grown sample. Since the sample was grown by hydrothermal method at relatively lower temperatures, it may contain some small number of preexisting defects, such as vacancies, interstitials, antisites, impurities (H and Li) or some extended defects. The sample quality can be further improved by postgrowth annealing at elevated temperatures. It was also found that the position of the main peak (002) shifted a little to the lower energy side after annealing at  $700$  and  $1000^\circ\text{C}$ . This indicates substitution of Co impurity in the ZnO lattice sites, which induces lattice expansion. Wang et al. [44] also observed that the peak position of X-ray diffraction shifted to the smaller angle due to substitution of implanted ions. For the  $\text{Co}^+$ -implanted ZnO before and after annealing up to  $1000^\circ\text{C}$ , no other peaks related to Co were observed in the XRD patterns. This suggests that no second phase such as Co metal clusters or Co metal oxides was generated in the sample. The local Co concentration in the as-implanted layer is 6 at.% according to the Monte Carlo simulation with maximum dose of  $1.25 \times 10^{17} \text{ cm}^{-2}$ . The solubility of Co in ZnO can be as high as 30 at.% [45]. So this concentration might be too low to form Co metal clusters. On the other hand, diffusion of the implanted Co ions will also happen during high-temperature annealing. This will further decrease the Co concentration, and the Co ion dissolves into ZnO and further replaces Zn. Park et al. [46] also found that in the Co-doped ZnO there was no sign of Co metal clusters or Co metal oxides when the content is lower than 12 at.%, and  $\text{Co}^{2+}$  automatically substitutes for  $\text{Zn}^{2+}$  in ZnO.

Figure 3 shows Raman spectra for the unimplanted, Co-implanted and thermally annealed ZnO

samples. For the wurtzite structure of ZnO, the expected collision/vibration modes are  $A_1+2E_2+E_1$ . The Raman-active phonon modes expected from group theory induce three vibration peaks in the Raman scattering spectrum [47]. In our measurement range of  $200\text{--}800 \text{ cm}^{-1}$ , these three peaks can all be observed, located at about  $331$ ,  $437$  and  $575 \text{ cm}^{-1}$ , respectively. The peak at  $331 \text{ cm}^{-1}$  is related to the second-order phonon ( $2E_2(\text{M})$ ). It barely changes after implantation and thermal treatment, [40] so it is not taken into account due to its stability. The predominant peak at about  $437 \text{ cm}^{-1}$  is the  $E_2$  (high) mode, which stands for the wurtzite structure of ZnO, while the peak at about  $575 \text{ cm}^{-1}$  corresponds to  $A_1$  (LO) or a defect-induced mode.

Comparing with the unimplanted ZnO, Co implantation does not induce destruction of the crystal structure of the sample, since the  $437 \text{ cm}^{-1}$  peak is only slightly affected, with some decrease in the peak intensity due to implantation damage. More distinct evidence of the implantation-induced defects is the significant heightening and broadening of the peak at  $575 \text{ cm}^{-1}$ . This peak is related to defects rather than the implanted Co, as the peak at the same position was reported in many other ion-implanted or even electron-irradiated ZnO [39, 40, 48].

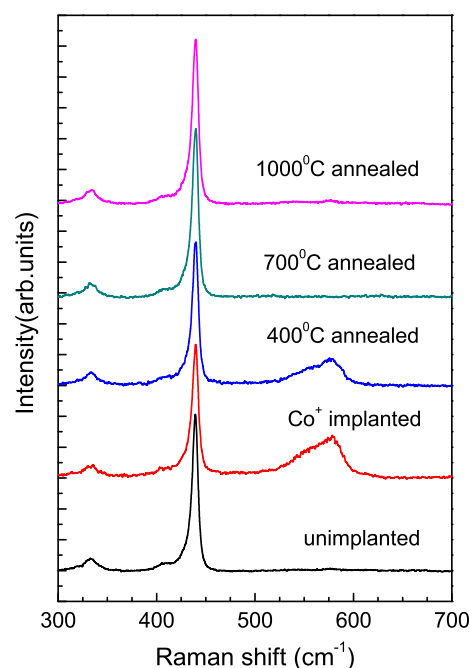


**Figure 3** Raman scattering spectra measured for ZnO before and after Co implantation and annealing at different temperatures.

Generally, the defect-induced modes are forbidden, but in defective crystals the Raman selection rules are relaxed, so these defect-induced modes appear. The implantation-induced defects cut the long-range lattice ordering, so the phonon frequencies close to the G point participate in the Raman scattering spectrum. Thus, a broad peak at  $575\text{ cm}^{-1}$  can be expected. The defects related to the  $575\text{ cm}^{-1}$  peak might be oxygen vacancies ( $V_O$ ) or Zn interstitials ( $Zn_i$ ), since this broad peak was also found in films grown in an oxygen-deficient condition [49–51].

After annealing the implanted sample at  $400\text{ }^\circ\text{C}$ , the broad peak shows only partial recovery. This means that the implanted defects, especially  $V_O$  related defects, remain stable up to  $400\text{ }^\circ\text{C}$ . After annealing at  $700\text{ }^\circ\text{C}$ , the broad peak recovers to the same level as the unimplanted sample. Accordingly, the  $E_2$  (high) mode at  $437\text{ cm}^{-1}$  also shows full recovery. This shows the same trend as the XRD results.

Doppler broadening  $S$  parameters as a function of incident positron energy  $E$  ( $S - E$  curve) measured for the unimplanted, Co-implanted and annealed ZnO are shown in Fig. 4. In the unimplanted single crystals, the  $S$  parameter exhibits a higher value at low incident energy and then decreases gradually with increasing positron energy and becomes constant at  $E > 5\text{ keV}$ . The higher  $S$  parameter is due to positron annihilation in the surface state. At lower incident positron energy, large fraction of positrons will diffuse back and get trapped at the surface. There are a lot of defects at the surface regions, which might be the reason for a relatively higher  $S$  parameter.

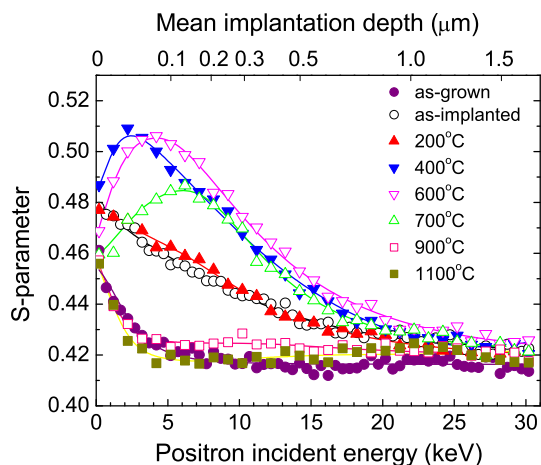


**Figure 4**  $S$ - $E$  curves measured for ZnO before and after Co implantation and annealing at different temperatures.

With increasing incident energy, positrons are implanted into deeper region, and the possibility of back diffusion becomes smaller, so the  $S$  parameter decreases gradually. When the positron energy is higher than  $5\text{ keV}$ , almost all the positrons annihilate in the deep bulk region, and the  $S$  parameter becomes constant.

After Co implantation, the  $S$  parameters at energies below  $20\text{ keV}$  all show a notable increase, which suggests introduction of defects by implantation. Most of the  $S$  parameters increase by more than 5% compared with the bulk  $S$  parameter in the unimplanted sample, indicating that most of the defects are vacancy clusters. However, we cannot exclude the existence of small vacancies such as Zn mono-vacancies, which coexist with vacancy clusters. Annealing of the implanted sample causes further increase in the  $S$  parameter. It can be seen that after annealing at  $200\text{ }^\circ\text{C}$ , the  $S$  parameter shows nearly no change. However, at  $400\text{ }^\circ\text{C}$ , the maximum  $S$  parameter at a positron energy of  $\sim 2\text{ keV}$  increases to 0.51, which is 22% higher than the bulk value. This implies that the vacancy clusters grow larger in size due to vacancy agglomeration. When the annealing temperature increases to  $600\text{ }^\circ\text{C}$ , the maximum  $S$  parameter in the  $S$ - $E$  curve shows nearly no change, but it shifts to positron energy of  $\sim 4\text{ keV}$ . Further increasing the annealing temperature to  $700\text{ }^\circ\text{C}$  causes decrease in the maximum  $S$  parameter, and the peak position shifts to  $\sim 6\text{ keV}$ . This may suggest that near-surface defects recover more easily. At an annealing temperature higher than  $700\text{ }^\circ\text{C}$ , the implantation-induced defects show fast recovery, and at  $1000$ – $1100\text{ }^\circ\text{C}$  all the implantation-induced

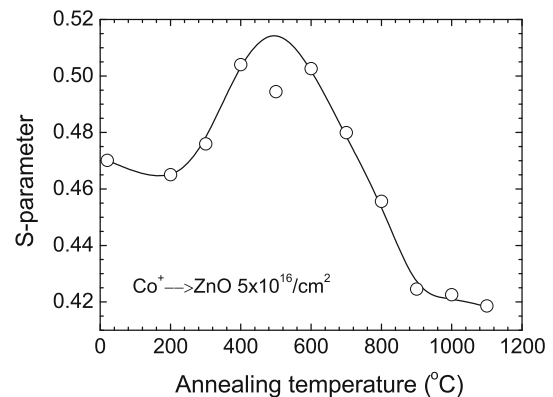


**Figure 5** Average  $S$  parameter in the damaged region as a function of annealing temperature for the Co-implanted ZnO. The solid line is a guide to the eye.

defects are removed, since the  $S - E$  curve is nearly the same as that of the unimplanted sample. We summed the Doppler broadening spectra measured in the central implanted region by choosing the corresponding positron energy range (which varies with annealing temperature as shown in Fig. 4), and calculated the average  $S$  parameter as a function of annealing temperature, which is shown in Fig. 5. From the figure, the variation of  $S$  parameters during annealing shows three stages. In the first stage (0–200 °C), the  $S$  parameter has nearly no change. With increasing annealing temperature, the  $S$  parameter shows continuous increase in the second stage (300–500 °C). This indicates growth of vacancy clusters. At higher temperatures, the small vacancies such as  $V_{Zn}$  and  $V_O$  become mobile and agglomerate into larger vacancy clusters. In the third stage (600–1100 °C), the  $S$  parameter begins to decrease, and it reaches almost the same value of the unimplanted sample at 1000–1100 °C, which implies gradual recovery of the vacancy clusters.

We also analyzed the correlation between the Doppler broadening  $S$  and  $W$  parameters ( $S - W$  curve) measured for the implanted sample after annealing at different temperatures. This analysis can provide more information about what goes on with defects during the annealing. Figure 6 shows the  $S - W$  data, and the data points can be fitted well by a straight line. This infers that the defect species have no apparent change. So no new defect species are produced during the annealing process, and only the respective concentration of each defects changes after annealing.

A comparison of the results obtained by XRD, Raman and positron annihilation measurements

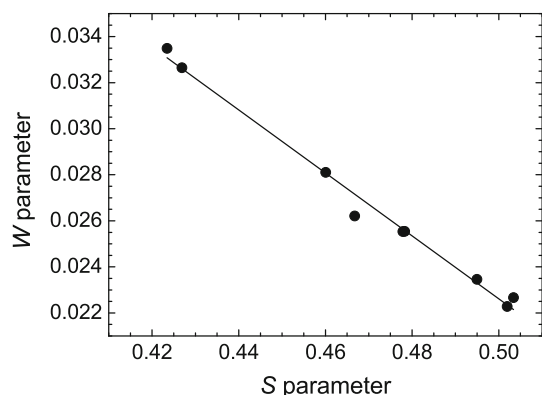


**Figure 6** The  $S - W$  correlation for the Co-implanted ZnO after annealing at different temperatures.

reveals that the above different methods detected different defect species in Co-implanted ZnO, since their thermal recovery processes are different. XRD and Raman scattering measurements all suggest that the implantation-induced damage can be recovered after annealing at about 700 °C. However, positron annihilation results indicate that a considerable amount of vacancy defects still remain after annealing at 700 °C. They can be fully removed only after annealing at 1000–1100 °C. This indicates that Zn vacancies and vacancy clusters have higher thermal stability than other defects induced by implantation, and positron annihilation spectroscopy is more sensitive than XRD and Raman Spectroscopy to the atomic-scale microstructure of materials.

The magnetic behavior of the Co-implanted ZnO was investigated by SQUID magnetization measurements. The unimplanted ZnO single crystal shows diamagnetism, so it was subtracted from the measured M-H curves. This also indicates that the small amount of preexisting defects in the as-grown ZnO have no apparent effect on the magnetic properties. Figure 7 shows the M-H curves of as-implanted, 700

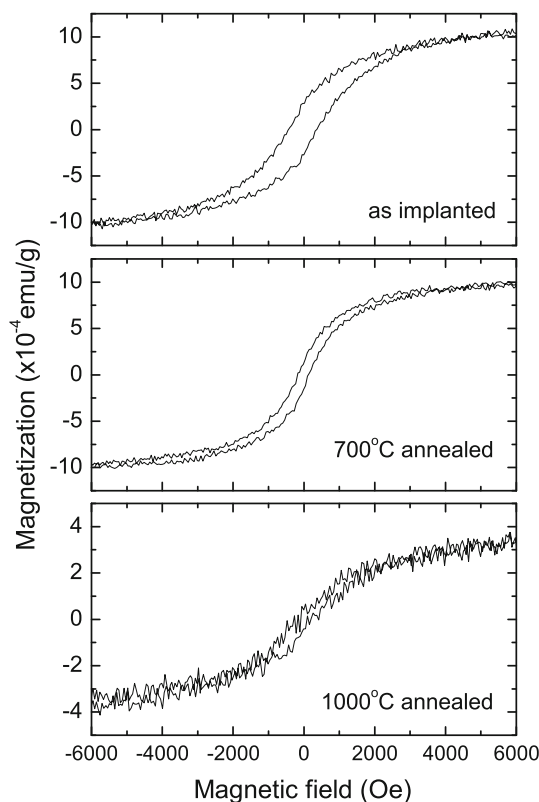


**Figure 7** M-H curves measured at 5 K for the Co-implanted ZnO sample before and after annealing.

and 1000 °C annealed ZnO measured at 5 K. All the samples show clear hysteretic loops at 5 K. The saturated magnetization for the as-implanted sample is about 0.0010 emu/g, and the coercivity is also as large as 400 Oe. After annealing the implanted sample at 700 °C, the saturated magnetization has nearly no change, while the coercivity shows a decrease. However, when the annealing temperature increases to 1000 °C, the saturated magnetization decreases to less than 0.0004 emu/g.

Since our XRD results indicate no signal related to Co clusters, the ferromagnetism is more probably due to the substitution of Zn by Co ions. However, it is interesting to find that the decrease in magnetization with increasing annealing temperature shows good correlation with the recovery of vacancy defects revealed by positron annihilation measurements. This gives us hints that the ferromagnetism is mediated by the vacancy defects. The implantation-induced defects will enhance the ferromagnetism caused by substitution of Co ions. Numerous works have been reported about the evidence of defect-related ferromagnetism in Co-doped ZnO [16, 18–20, 22, 23]. The problem is that there is no agreement on the defect species which is responsible for the enhanced magnetization. Most of the reports claim that the ferromagnetism is mediated by O vacancies, [16, 19, 20, 23] while some others suggest that Zn vacancies or O interstitials might enhance the ferromagnetism [22]. The reason for this contradictory result is that there is a lack of an appropriate method to clarify the vacancy defects in ZnO. Some of the experimental works used postgrowth annealing in different atmosphere such as air or argon to create or annihilate O vacancies and come to the conclusion that the ferromagnetism is induced by O vacancies. Others used conventional methods such as photoluminescence to discriminate oxygen vacancies. All these methods cannot give clear proof of oxygen vacancies. In contrast, positron annihilation is particularly sensitive to vacancies. In ZnO, oxygen vacancies are invisible to positrons, [42] so positrons can only detect Zn vacancies and vacancy clusters. According to our positron annihilation and magnetization measurements for Co-implanted ZnO, Zn vacancies and vacancy clusters are possible candidates for the enhancement of ferromagnetism.

In order to confirm the mediation of magnetization by vacancies, spin-polarized calculations are performed by using Vienna Ab-initio Simulation

Package (VASP) based on density functional theory. As shown in Fig. 8, we employ a 3\*3\*2 super cell to simulate the doped system, which contains 34 Zn, 36 O atoms and two Co atoms which occupy the Zn lattice sites, named as ZnO:Co. Comparing with the pure ZnO system, [52] ferromagnetism can be induced by the two impurity atoms, which is in accordance with the previous study [53]. The magnetic moment is about 6.20  $\mu_B$ , which is slightly larger than 6.0  $\mu_B$  for the system with the defect complex consisting of Co dopants and  $V_O$ . Figure 9a–c shows the spin-polarized density of states (DOS) distribution of ZnO:Co system; it can be seen that the Co-3d and O-2p states around the Fermi level are spin-

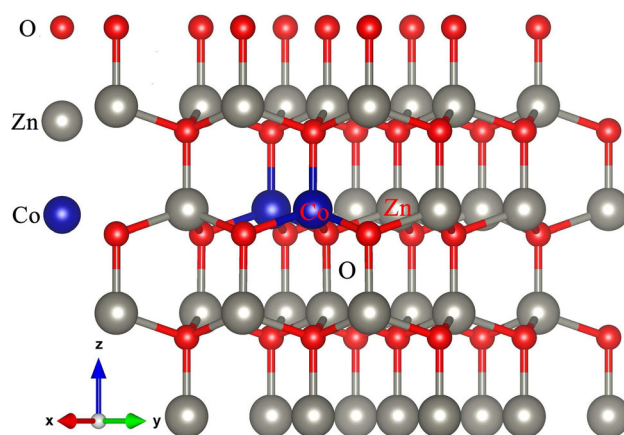


**Figure 8** Configuration of doped ZnO system with two Co atoms. Red, gray and blue spheres designate O, Zn and Co atoms, respectively.

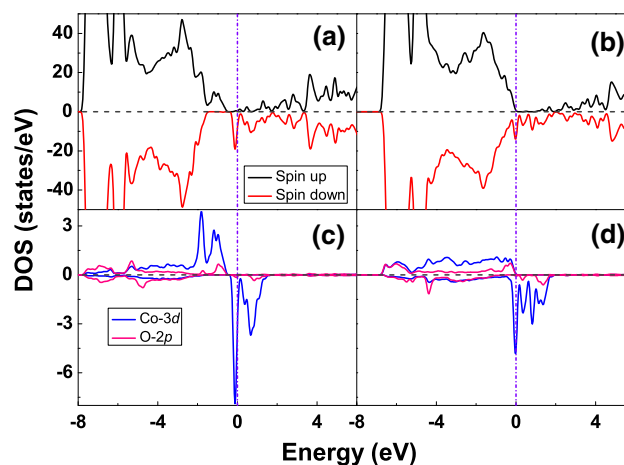


**Figure 9** Total density of states (DOS) for (a) Co-doped ZnO and (b) Co-doped ZnO with Zn vacancy; partial density of states (PDOS) for (c) Co-doped ZnO and (d) Co-doped ZnO with Zn vacancy.

polarized and hybridize strongly with each other, which results in the ferromagnetism in this system [53]. However, the value of magnetic moment increases to  $8.0 \mu_B$  when the Zn vacancy exists near Co impurity atoms ( $\text{ZnO:Co}+V_{\text{Zn}}$ ). Comparing with the DOS of the ZnO:Co system, more impurity levels appear at the bottom of conduction band in ZnO:Co+ $V_{\text{Zn}}$  system (Fig. 9b), which are mainly derived from the contributions of the Co-3d and O-2p states highly coupled with each other. For vacancy clusters near the Co impurities, we found that as long as the vacancy cluster contains excessive Zn monovacancies, it has almost the same effect as that of Zn monovacancies. For example, the vacancy cluster  $V_{\text{Zn-O-Zn}}$  near Co impurity will produce magnetic moment of  $7.64 \mu_B$ . Therefore, strong interaction between impurity Co atoms and adjacent O atom may be the reason of ferromagnetic enhancement in these systems.

## Conclusion

Co ions with multiple energies were implanted into ZnO single crystals. XRD patterns indicate no Co cluster or other second-phase formation in the implanted layer. After annealing, Co ions are distributed in the Zn lattice site. XRD and Raman scattering spectra all indicate implantation-induced damage, and it shows full recovery after annealing at around  $700^\circ\text{C}$ . However, positron annihilation Doppler broadening measurements reveal that most of the implantation-induced defects still exist after annealing at  $700^\circ\text{C}$ . They are annealed out only after high-temperature annealing at  $1000\text{--}1100^\circ\text{C}$ . The implanted sample shows clear ferromagnetism measured at 5 K. The magnetization shows nearly no change after annealing at  $700^\circ\text{C}$ , and a large decrease after annealing at  $1000^\circ\text{C}$ . It is clear that the ferromagnetism in Co-doped ZnO is mediated by defects, such as the implantation-induced Zn vacancies or vacancy clusters. The strong hybridization between Co-3d and O-2p states is the possible reason for the enhanced ferromagnetism by Zn-related vacancies.

## Acknowledgements

This work was supported by the National Natural Science Foundation of China under Grant Nos.

11305117, 11475130 and 11575131 and by Henan University of Science and Technology (Grant No. 2015GJB014).

## References

- [1] Chambers SA (2002) A potential role in spintronics. *Mater Today* 5:34–39
- [2] Punnoose A, Reddy KM, Hays J, Thurber A (2006) Magnetic gas sensing using a dilute magnetic semiconductor. *Appl Phys Lett* 89:112509
- [3] Dietl T, Ohno H, Matsukura F, Cibert J, Ferrand D (2000) Zener model description of ferromagnetism in zinc-blende magnetic semiconductors. *Science* 287:1019–1022
- [4] Pearton SJ, Abernathy CR, Overberg ME, Thaler GT, Norton DP, Theodoropoulou N, Hebard AF, Park YD, Ren F, Kim J (2003) Wide band gap ferromagnetic semiconductors and oxides. *J Appl Phys* 93:1–13
- [5] Alaria J, Bieber H, Colis S, Schmerber G, Dinia A (2006) Absence of ferromagnetism in Al-doped Zn<sub>0.9</sub>Co<sub>0.100</sub> diluted magnetic semiconductors. *Appl Phys Lett* 88:112503
- [6] Theodoropoulou N, Hebard AF, Overberg ME, Abernathy CR, Pearton SJ, Chu SNG, Wilson RG (2001) Magnetic and structural properties of Mn-implanted GaN. *Appl Phys Lett* 78:3475–3477
- [7] Majid A, Sharif R, Husnain G, Ali A (2009) Annealing effects on the structural optical and magnetic properties of Mn implanted GaN. *J Phys D Appl Phys* 42:135401–135409
- [8] Sharma VK, Varma GD (2009) Effect of Al and Sb doping on the magnetic properties of ZnMnO and ZnCoO. *J Appl Phys* 105:07C510
- [9] Ueda K, Tabata H, Kawai T (2001) Magnetic and electric properties of transition-metal-doped ZnO films. *Appl Phys Lett* 79:988–990
- [10] Schwartz DA, Gamelin DR (2004) Reversible 300 K ferromagnetic ordering in a diluted magnetic semiconductor. *Adv Mater* 16:2115–2119
- [11] Wang Q, Sun Q, Chen G, Kawazoe Y, Jena P (2008) Vacancy-induced magnetism in ZnO thin films and nanowires. *Phys Rev B Condens Matter* 77:205411
- [12] Zuo X, Yoon SD, Yang A, Duan WH, Vittoria C, Harris VG (2009) Ferromagnetism in pure wurtzite zinc oxide. *J Appl Phys* 105:07C508
- [13] Gao D, Zhang Z, Fu J, Xu Y, Qi J, Xue D (2009) Room temperature ferromagnetism of pure ZnO nanoparticles. *J Appl Phys* 105:113928
- [14] Liu W, Li W, Hu Z, Tang Z, Tang X (2011) Effect of oxygen defects on ferromagnetic of undoped ZnO. *J Appl Phys* 110:123911

- [15] Zhan P, Xie Z, Li Z, Wang W, Zhang Z, Li Z, Cheng G, Zhang P, Wang B, Cao X (2013) Origin of the defects-induced ferromagnetism in un-doped ZnO single crystals. *Appl Phys Lett* 102:071914
- [16] Hsu HS, Huang JCA, Huang YH, Liao YF (2006) Evidence of oxygen vacancy enhanced room-temperature ferromagnetism in Co-doped ZnO. *Appl Phys Lett* 88:242507
- [17] Yan WS, Sun Z, Liu Q, Li Z, Pan Z, Wang J, Wei S, Wang D, Zhou Y, Zhang X (2007) Zn vacancy induced room-temperature ferromagnetism in Mn-doped ZnO. *Appl Phys Lett* 91:062113
- [18] Liu EZ, Jiang JZ (2010) O-vacancy-mediated spin-spin interaction in Co-doped ZnO: first-principles total-energy calculations. *J Appl Phys* 107:023909
- [19] Yan WS, Jiang QH, Sun ZH, Yao T, Hu FC, Wei SQ (2010) Determination of the role of O vacancy in Co:ZnO magnetic film. *J Appl Phys* 108:013901
- [20] Gu H, Zhang W, Xu Y, Yan M (2012) Effect of oxygen deficiency on room temperature ferromagnetism in Co doped ZnO. *Appl Phys Lett* 100:202401
- [21] Liu WJ, Tang XD, Tang Z (2013) Effect of oxygen defects on ferromagnetism of Mn doped ZnO. *J Appl Phys* 114:123911
- [22] Ren HT, Xiang G, Gu G, Zhang X (2014) Enhancement of ferromagnetism of ZnO: Co nanocrystals by post-annealing treatment: the role of oxygen interstitials and zinc vacancies. *Mater Lett* 122:256–260
- [23] Simimol A, Anappara AA, Greulich-Weber S, Chowdhury P, Barshilia HC (2015) Enhanced room temperature ferromagnetism in electrodeposited Co-doped ZnO nanostructured thin films by controlling the oxygen vacancy defects. *J Appl Phys* 117:214310
- [24] Shao Q, Wang C, Zapfen JA, Leung CW, Ruotolo A (2015) Ferromagnetism in Ti-doped ZnO thin films. *J Appl Phys* 117:17B908
- [25] Li XL, Wang ZL, Qin XF, Wu HS, Xu XH, Gehring GA (2008) Enhancement of magnetic moment of Co-doped ZnO films by postannealing in vacuum. *J Appl Phys* 103:023911
- [26] Lee HJ, Jeong SY, Cho CR, Park CH (2002) Study of diluted magnetic semiconductor: Co-doped ZnO. *Appl Phys Lett* 81:4020–4022
- [27] Rode K, Anane A, Mattana R, Contour JP, Durand O, Lebourgeois R (2003) Magnetic semiconductors based on cobalt substituted ZnO. *J Appl Phys* 93:7676–7678
- [28] Lawes G, Risbud AS, Ramire AP, Seshadri R (2005) Absence of ferromagnetism in Co and Mn substituted polycrystalline ZnO. *Phys Rev B* 71:045201
- [29] Zhang Z, Chen Q, Lee HD, Xue YY, Sun YY, Chen H, Chen F, Chu WK (2006) Absence of ferromagnetism in Co-doped ZnO prepared by thermal diffusion of Co atoms. *J Appl Phys* 100:043909
- [30] Yin S, Xu MX, Yang L, Liu JF, Rosner H, Hahn H, Gleiter H, Schild D, Doyle S, Liu T, Hu TD, Takayama-Muromachi E, Jiang JZ (2006) Absence of ferromagnetism in bulk polycrystalline Zn<sub>0.9</sub>Co<sub>0.1</sub>O. *Phys Rev B* 73:224408
- [31] de Carvalho HB, de Godoy MPF, Paes RWD, Mir M, Ortiz de Zevallos A, Iikawa F, Brasil MJSP, Chitta VA, Ferraz WB, Boselli MA, Sabioni ACS (2010) Absence of ferromagnetic order in high quality bulk Co-doped ZnO samples. *J Appl Phys* 108:033914
- [32] Norton DP, Overberg ME, Pearton SJ, Pruessner K, Budai JD, Boatner LA, Chisholm MF, Lee JS, Khim ZG, Park YD (2003) Ferromagnetism in cobalt-implanted ZnO. *Appl Phys Lett* 83:5488–5490
- [33] Potzger K, Zhou S, Reuther H, Mucklich A, Eichhorn F, Schell N, Skorupa W, Helm M, Fassbender J, Herrmannsdorfer T (2006) Fe implanted ferromagnetic ZnO. *Appl Phys Lett* 88:052508
- [34] Wu P, Saraf G, Lu Y, Hill DH, Gateau R, Wielunski L, Bartynski RA, Arena DA, Dvorak J, Moodenbaugh A (2006) Ferromagnetism in Fe-implanted a-plane ZnO films. *Appl Phys Lett* 89:012508
- [35] Zhou SQ, Potzger K, Borany JV, Grotzschel R, Skorupa W, Helm M, Fassbender J (2008) Crystallographically oriented Co and Ni nanocrystals inside ZnO formed by ion implantation and postannealing. *Phys Rev B* 77:035209
- [36] Schumm M, Koerdel M, Muller S, Ronning C, Dynowska E, Golacki Z, Szuskiewicz W, Geurts J (2009) Secondary phase segregation in heavily transition metal implanted ZnO. *J Appl Phys* 105:083525
- [37] Wikberg JM, Knut R, Audren A, Ottosson M, Linnarsson MK, Karis O, Hallen A, Svedlindh P (2011) Annealing effects on structural and magnetic properties of Co implanted ZnO single crystals. *J Appl Phys* 109:083918
- [38] Srivastava P, Ghosh S, Joshi B, Satyarthi P (2012) Probing origin of room temperature ferromagnetism in Ni ion implanted ZnO films with x-ray absorption spectroscopy. *J Appl Phys* 111:013715
- [39] Chen ZQ, Wang SJ, Maekawa M, Kawasuso A, Naramoto H, Yuan XL, Sekiguchi T (2007) Thermal evolution of defects in as-grown and electron-irradiated ZnO studied by positron annihilation. *Phys Rev B* 75:245206
- [40] Chen ZQ, Kawasuso A, Xu Y, Naramoto H, Yuan XL, Sekiguchi T, Suzuki R, Ohdaira T (2005) Microvoid formation in hydrogen-implanted ZnO probed by a slow positron beam. *Phys Rev B* 71:115213
- [41] Chen ZQ, Maekawa M, Yamamoto S, Kawasuso A, Yuan XL, Sekiguchi T, Suzuki R, Ohdaira T (2004) Evolution of

- voids in Al-implanted ZnO probed by a slow positron beam. *Phys Rev B* 69:035210
- [42] Tuomisto F, Ranki V, Saarinen K, Look DC (2003) Evidence of the Zn vacancy acting as the dominant acceptor in n-type ZnO. *Phys Rev Lett* 91:205502
- [43] Biersack JP, Haggmark LG (1980) A Monte Carlo computer program for the transport of energetic ions in amorphous targets. *Nucl Instrum Methods* 174(1–2):257–269
- [44] Wang XB, Song C, Geng KW, Zeng F, Pan F (2006) Luminescence and Raman scattering properties of Ag-doped ZnO films. *J Phys D Appl Phys* 39:4992–4996
- [45] Mandal SK, Das AK, Nath TK, Karmakar D (2006) Temperature dependence of solubility limits of transition metals (Co, Mn, Fe, and Ni) in ZnO nanoparticles. *Appl Phys Lett* 89:144105
- [46] Park JH, Min GK, Jang HM, Ryu S, Kim YM (2004) Co-metal clustering as the origin of ferromagnetism in Co-doped ZnO thin films. *Appl Phys Lett* 84:1338–1340
- [47] Damen TC, Porto SPS, Tell B (1966) Raman effect in zinc oxide. *Phys Rev* 142:570–574
- [48] Chen ZQ, Kawasuso A, Xu Y, Naramoto H (2005) Production and recovery of defects in phosphorus-implanted ZnO. *J Appl Phys* 97:013528
- [49] Zeng JN, Low JK, Ren ZM, Liew T, Lu YF (2002) Effect of deposition conditions on optical and electrical properties of ZnO films prepared by pulsed laser deposition. *Appl Surf Sci* 197–198:362–367
- [50] Jeong S-H, Kim J-K, Lee B-T (2003) Effects of growth conditions on the emission properties of ZnO films prepared on Si (100) by rf magnetron sputtering. *J Phys D Appl Phys* 36:2017
- [51] Youn CJ, Jeong TS, Han MS, Kim JH (2004) Optical properties of Zn-terminated ZnO bulk. *J Cryst Growth* 261:526–532
- [52] Zhang T, Song L, Chen Z, Shi E, Chao L, Zhang H (2006) Origin of ferromagnetism of (Co, Al)-codoped ZnO from first-principles calculations. *Appl Phys Lett* 89:172502
- [53] Hu S, Yan S, Zhao M, Mei L (2006) First-principles LDA+U calculations of the Co-doped ZnO magnetic semiconductor. *Phys Rev B* 73:245205